Ultra-compact all-in-fiber-core Mach-Zehnder interferometer

PENGCHENG CHEN[1], XUEWEN SHU[1,*], KATE SUGDEN[2]

[1] *Wuhan National Laboratory for Optoelectronics & School of Optoelectronic Science and Engineering, Huazhong University of Science and Technology, Wuhan 430074, China*
[2] *Aston Institute of Photonic Technologies, Aston University, Birmingham B4 7ET, UK*

** Corresponding author: xshu@hust.edu.cn*

Received XX Month XXXX; revised XX Month, XXXX; accepted XX Month XXXX; posted XX Month XXXX (Doc. ID XXXXX); published XX Month XXXX

Optical Mach-Zehnder interferometers (MZI) are useful components in a variety of optical applications including: optical modulation; signal processing; and physical, chemical, and biological sensing. We introduce here a novel, assembly-free all-in-fiber-core MZI, which is directly written with a femtosecond laser. By introducing a positive refractive index-modified zone (PRIMZ) in half of the fiber core, the original single-moded fiber section is converted into a few-moded fiber section, where a strong coupling between the two lowest-order guided modes is generated, resulting in a well-defined interference spectrum in transmission. This device promises many significant advantages over existing approaches such as: ease of fabrication; stability; small insertion loss; robustness; extremely broad operating bandwidth, and precise and controllable cavity lengths. These advantages make this device strikingly attractive with the potential for extensive adoption in fiber communications, signal processing, sensors and laser wavelength control. © 2017 Optical Society of America

OCIS codes: *(230.1150) All-optical devices. (060.0060) Fiber optics and optical communications; (220.0220) Optical design and fabrication; (230.0230) Optical devices; (230.4000) Microstructure fabrication; (060.2370)*

http://dx.doi.org/10.1364/OL.99.099999

Optical Mach-Zehnder interferometers (MZI) are useful components in a variety of optical applications including: optical nodulation; signal processing; and physical, chemical, and biological sensing[1-6]. An in-fiber MZI is particularly notable for its stability, low loss and multiplexing capability.

Various types of in-fiber MZI configurations have been proposed including: a pair of long period fiber gratings (LPGs)[7]; segment fusing of specialty fiber[6, 8, 9]; microfiber-based structures[3, 10]; mode field or core-mismatch fusion splice[11, 12]; and in-fiber air cavities[13]. All of these options have disadvantages. For example, LPGs require precise fabrication, are sensitive to temperature, and the interference spectrum range is limited by the LPG bandwidth. Specialty fiber is expensive and only a few of the designs result in high-contrast stripes. Fiber core lateral mismatch or mode field fusion is hard to achieve with good reproducibility since it requires the time-consuming manual assembly of pieces of fiber. Microfiber and air cavity devices are inherently fragile with poor robustness. The above-mentioned configurations are based on core-cladding modes interference, which usually have a complicated, uneven interference spectrum and high insertion loss. In addition, due to the fact that the cladding modes are susceptible to external surrounding disturbance, they are unsuitable for optical communication and signal processing applications, and usually, as sensors, cladding interferometers have strong crosstalk between temperature, bending, refractive index and strain. Furthermore, their free spectral range is difficult to precisely control.

Fiber in-line MZIs have previously been demonstrated using direct femtosecond micromachining inscription [14]. However, the published structures had poor mechanical properties and large insertion loss. Aside from ablation from a high-energy fs-laser, fs-lasers can be used to create permanent positive or negative refractive index modifications in a localized region inside the material. Since the discovery of this effect, numerous devices have been demonstrated, such as: optical waveguides [15]; Bragg grating waveguides [16]; directional couplers [17], and photonic crystals [18]. This approach to forming waveguides has opened up a new avenue in producing three-dimensional integrated optical circuits in a single writing step, however, most of previous studies are focused on bulk materials which then require precise 3D assembly that present significant processing challenges in forming integrated photonic components. Fortunately, optical fiber may be a perfect host material due to its inherent compact size, low cost and compatibility with existing optical communication systems.

In this paper, a compact, assembly-free, all-in-fiber-core MZI is proposed and demonstrated using direct femtosecond (fs) laser inscription. The novel design approach potentially offers

significant advantages including: simple fabrication: low insertion loss; high robustness; high-contrast fringes;, flat spectra, and a wide range of precisely controllable cavity lengths.

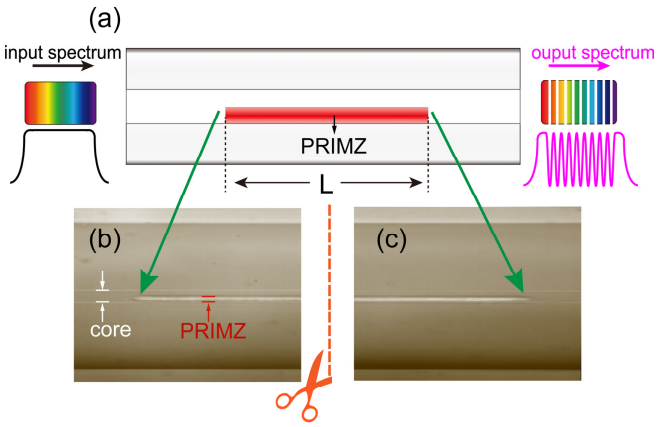

Fig. 1 (**a**) Schematic diagram of the proposed all-in-fiber-core MZI. (**b**)(**c**) The microscope images of the fabricated MZI near two ends.

Figure 1 shows the schematic diagram of the proposed all-in-fiber-core MZI, the key structure of which is an off-axial positive refractive index-modified zone (PRIMZ). The PRIMZ is created by direct femtosecond laser inscription modifying the refractive index of part of the core along length *L*. Introducing the PRIMZ converts the original single-moded fiber section into a few-moded fiber section. Thus, when the incident light propagates through the few-mode fiber section, an optical path difference (OPD) can be obtained due to the effective refractive index difference between different modes. The interference between these modes forms an MZI.

The phase difference between the fundamental mode and a higher-order mode after propagating through the length L of the modified fiber can be approximated to:

$$\varphi = \frac{2\pi \cdot OPD}{\lambda} = \frac{2\pi \cdot \Delta n_{eff} L}{\lambda} \quad (1)$$

where Δn_{eff} is the effective refractive index difference between the fundamental mode and the higher-order mode, and λ is the wavelength of light in vacuum. When the phase difference satisfies the condition $\varphi = (2m+1)\pi$, and where m is an integer, an intensity dip appears at wavelengths:

$$\lambda_m = \frac{2\Delta n_{eff} L}{2m+1} \quad (2)$$

The free spectral range (FSR) of the interference fringe pattern is determined by the OPD, $\Delta n_{eff} L$, such that:

$$FSR = \frac{\lambda^2}{\Delta n_{eff} L} \quad (3)$$

The FSR determines the density of the comb-like transmission spectra.

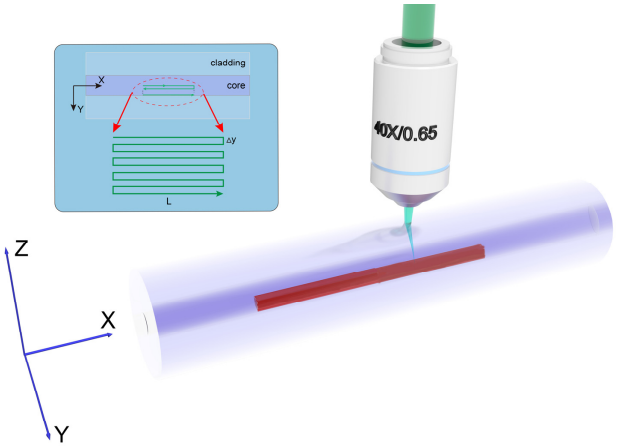

Fig. 2. Setup for direct writing PRIMZ in the SMF core by fs-laser. **Insert:** the scanning track of the fs-laser in the SMF core.

The setup used for the direct fs-laser writing of the PRIMZ in the SMF is shown in Fig. 2. The repetition rate, central wavelength, and pulse width were 200kHz, 520nm, and 350fs, respectively. The fabrication process of the proposed all-in-fiber-core MZI involves only this one step. The laser beam was directed into an objective lens (Olympus UMPLFL 40X) with a numerical aperture (NA) of 0.65. The single mode optical fiber (YOFC) with a core/cladding diameter of ~8/125μm was mounted on a computer-controlled XYZ translation stage (Newport, Inc.) with a resolution of 0.02μm, in parallel with the x-axis. For the inscription, the center of the fiber core was first positioned at the focal point of the fs-laser, then the stage was translated so that the laser focus was scanned in the XY plane following the path illustrated in the insert of Fig. 2. The separation between each scanned track was 0.5μm (Δy) and the scan speed was 200μm/s. The single pulse energy before the objective lens was about 0.6μJ. As a result of the exposure, a straight in-core PRIMZ was introduced, the optical microscope images of the PRIMZ of one sample was shown in Fig. 1(b) and (c).

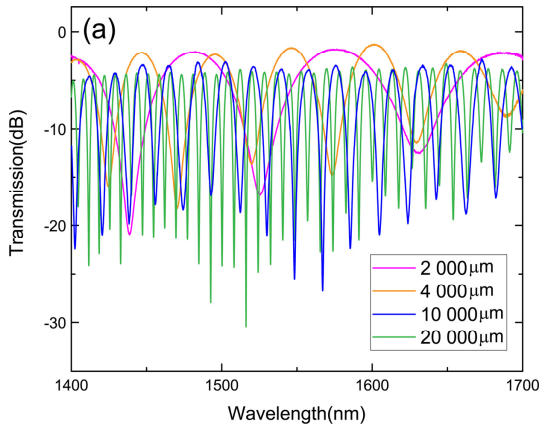

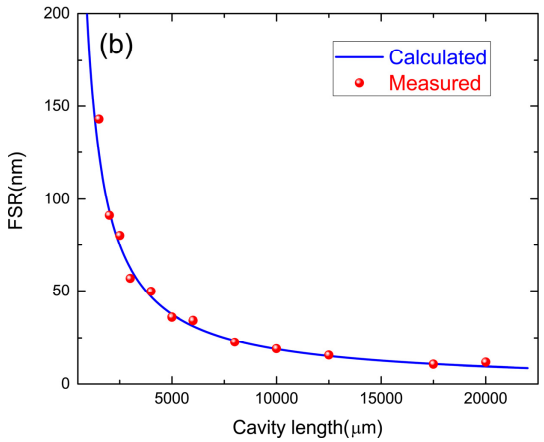

Fig.3. (**a**) Transmission spectra of the MZIs with different PRIMZ lengths. (**b**) Measured and calculated FSR of interference fringes of the device.

A series of samples were fabricated with different PRIMZ lengths and their spectral response in transmission measured using a supercontinuum white-light source (YSL Supercontinuum Source SC-5) and an optical spectrum analyzer (OSA, YOKOGAWA AQ6370C) with the 0.02nm spectral resolution. Figure 3(a) shows four MZIs with different PRIMZ lengths of 2000, 4000, 10000 and 20000μm, respectively. The insertion losses are flat across the full 300nm range measured and increase as the PRIMZ length increases. The devices with PRIML lengths of 2000μm and 4000μm have an insertion loss of about 3dB with a fringe visibility of nearly 20dB. The longer PRIMZ length corresponds to the larger insertion loss. When the PRIMZ becomes longer, the light suffers more scattering and diffraction and it is believed this is contributing to the additional loss. Based on the measured FSR and Eq. (3), we can estimate that the fs-laser induced refractive-index increase (Δn_{eff}) in the SMF is approximately 0.011.

Eq. (3) indicates that the FSR is inversely proportional to the length of the cavity (PRIMZ), and so can be controlled during fabrication. To experimentally verify this relationship, a number of MZIs were fabricated with different PRIMZ lengths. The measured FSRs of the samples are shown in Fig. 3(b) and show a good agreement with the calculated values.

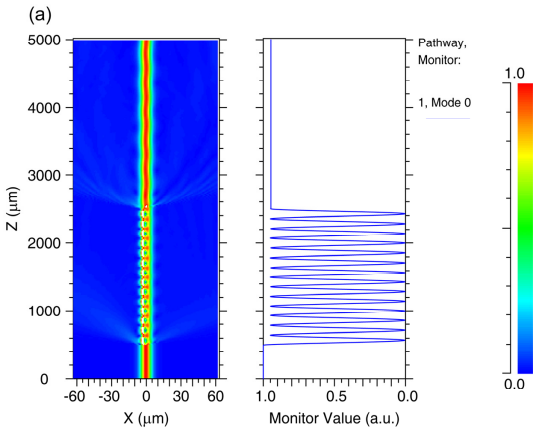

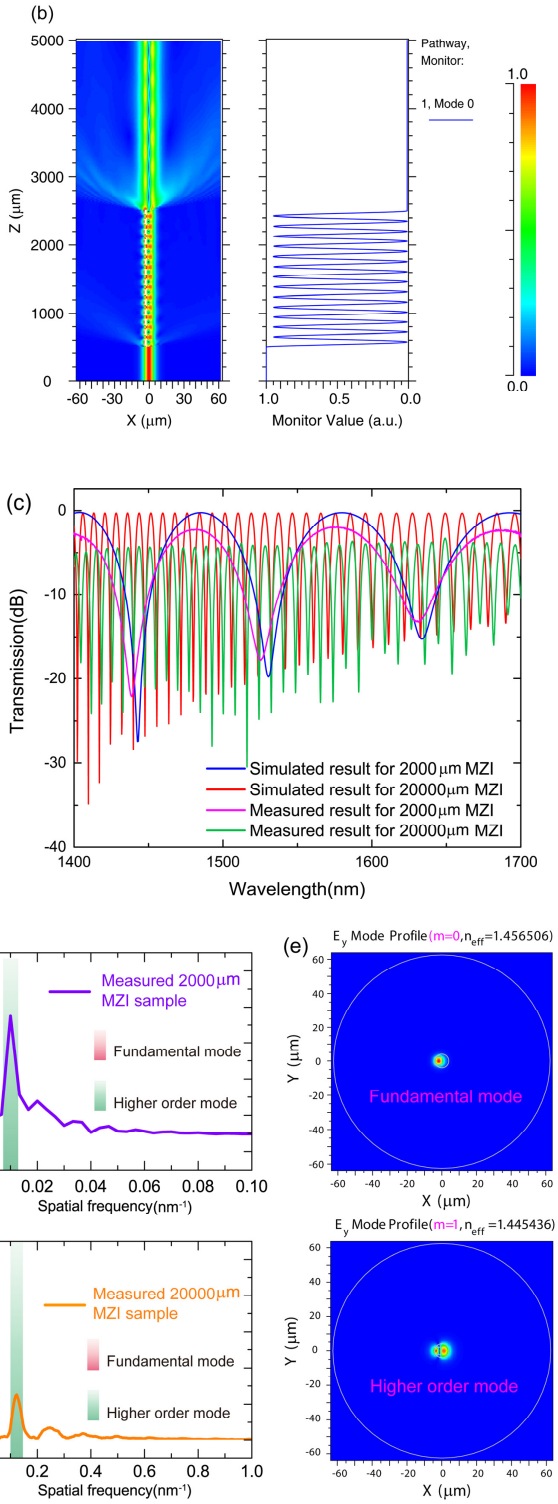

Fig. 4. (**a**) and (**b**) The propagation field distribution and the normalized propagating power along the MZI with cavity length 2000μm at input wavelength of 1485nm and 1530nm, respectively. (**c**) The simulated and measured results with cavity length of 2000μm and 20000μm, respectively. (**d**) Spatial frequency spectra taken by FFT with measured cavity length of 2000μm and 20000μm, respectively. (**e**) The simulated mode field patterns of the structure.

The structure was simulated using a beam propagation method (BPM) to analyze the light propagating through the SMF and MZI region. Figures 4(a) and (b) show the simulated propagation field distribution and the normalized propagating power along a 2000μm long MZI; the wavelengths used were chosen to show the difference between the low and high loss regions of the transmission spectra. Figure 4(a) shows the simulation with an input wavelength at 1485nm (a construtive interference peak). It is apparent that the light after the MZI is tightly confined in the fiber core and there is almost no light power loss. Figure 4(b) shows a simulation with input wavelength at 1530nm (an interference dip), from which we can see that the light field after the interference is no longer confined to the fiber core, but widely spreads into the cladding area. Evidently, one can see strong mode coupling in the PRIMZ section from both Fig. 4(a) and (b). Figure 4(c) presents the simulated and measured transmission spectra of two MZI structures with cavity length of 2000μm and 20000μm, respectively. The measured results show a good agreement with the theoretical predictions. The discrepancy between the simulated and measured results could be due to the roughness of the PRIMZ surfaces and also likely a small difference between the simulation and actual values of Δn_{eff} . To further analyze the number and the power distribution of the interference modes, we perform the corresponding Fast Fourier transform (FFT) spectra of the measured MZIs with cavity length of 2000μm and 20000μm, respectively, as shown in Fig. 4(d). Obviously, the interference is dominated by two modes: one fundamental mode and one higher-order mode. The propagating modes in the modified structure are were simulated using BPM. Figure 4(e) shows the computed mode patterns of the two guided core modes at a wavelength of 1550nm. Due to the introducing of the PRIMZ, the mode field distribution in the modified section is significant different to that in conventional SMF. It is clearly seen that one guided mode is confined in the PRIMZ (we call it the fundamental mode since it has the highest effective refractive index) while a higher-order guided mode is mainly confined in the remaining core area. The MZI effect is dominated by the interference of these two modes.

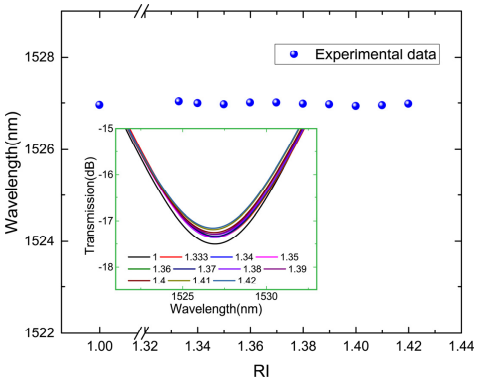

Fig. 5. Responses of the device to surrounding RI.

In addition, the response of the MZI to the surrounding RI (SRI) was investigated. Fig. 5 shows that the center wavelength of the 1527nm dip of the MZI barely changes when the SRI is increased from 1 to 1.44, thus the device is believed to be insensitive to the SRI due to the fact that the modal interference is mainly contained within the fiber core. This feature is very advantageous for device packaging and overall stability. We also measured the temperature response of the proposed MZI, which has a temperature sensitivity of 12.6pm/ °C .

In summary, we report an integrated assembly-free all-in-fiber-core MZI based on direct, single-step, fs-laser writing. This new device is a very promising candidate for many aspects of photonics applications. This novel work has potentially significant ramifications in optical communications and signal processing. The design can be applied to a number of applications such as switching, optical add/drop multiplexing (OADM), comb filtering, variable optical attenuation, signal modulation/demodulation, optical differentiators, format conversion, all-fiber lasers, tunable devices and optical sensors. The simplicity of the fabrication leads to a decreased component cost and is coupled with high performance and easy integration. We believe that such a directly-written in-fiber-core MZI can be an important building block for future integrated "all-in-a-fiber" photonics circuits and network.

Funding. National Natural Science Foundation of China (NSFC) (61775074); National 1000 Young Talents Program, China; 111 Project (No. B07038); Natural Science Foundation of Guangdong Province, China (2015A030313633)

Acknowledgment. The authors thank Prof. M. Sumetsky for his useful discussion.

References

1. X. Lei, B. C. Wang, V. Baby, I. Glesk, and P. R. Prucnal, IEEE Photo. Techno. Lett. **15**, 308 (2003).
2. H. Chi, Z. Li, X. Zhang, S. Zheng, X. Jin, and J. P. Yao, Opt. Lett. **36**, 1629 (2011).
3. R. Yang, Y. S. Yu, Y. Xue, C. Chen, Q. D. Chen, and H. B. Sun, Opt. Lett. **36**, 4482 (2011).
4. Y. Xu, P. Lu, Z. Qin, J. Harris, F. Baset, P. Lu, V. R. Bhardwaj, and X. Bao, Opt. Express **21**, 3031 (2013).
5. J. Zhou, C. Liao, Y. Wang, G. Yin, X. Zhong, K. Yang, B. Sun, G. Wang, and Z. Li, Opt. Express **22**, 1680 (2014).
6. L. V. Nguyen, D. Hwang, S. Moon, D. S. Moon, and Y. Chung, Opt. Express **16**, 11369 (2008).
7. H. Fu, X. Shu, A. Zhang, W. Liu, L. Zhang, S. He, and I. Bennion, IEEE Sens. J. **11**, 2878 (2011).
8. H. Y. Choi, M. J. Kim, and B. H. Lee, Opt. Express **15**, 5711 (2007).
9. Y. Jung, S. Lee, B. H. Lee, and K. Oh, Opt. Lett. **33**, 2934 (2008).
10. Y. Xue, Y. S. Yu, R. Yang, C. Wang, C. Chen, J. C. Guo, X. Y. Zhang, C. C. Zhu, and H. B. Sun, Opt. Lett. **38**, 1209 (2013).
11. D.-W. Duan, Y.-J. Rao, L.-C. Xu, T. Zhu, D. Wu, and J. Yao, Sens. Actuators B: Chem. **160**, 1198 (2011).
12. L. Mao, P. Lu, Z. Lao, D. Liu, and J. Zhang, Opt Laser Technol. **57**, 39 (2014).
13. P. Minkyu, L. Sejin, H. Woosung, K. Dae-Kyu, S. Woojin, S. Ik-Bu, and O. Kyunghwan, IEEE Photo. Techno. Lett. **21**, 1027 (2009).
14. Y. Wang, M. Yang, D. N. Wang, S. Liu, and P. Lu, J. Opt. Soc. Am. B. **27**, 370 (2010).
15. K. M. Davis, K. Miura, N. Sugimoto, and K. Hirao, Opt. Lett. **21**, 1729 (1996).
16. H. Zhang, S. M. Eaton, J. Li, and P. R. Herman, Opt. Lett. **31**, 3495 (2006).
17. L. A. Fernandes, J. R. Grenier, P. R. Herman, J. S. Aitchison, and P. V. Marques, Opt. Express **19**, 11992 (2011).
18. T. Kondo, S. Matsuo, S. Juodkazis, and H. Misawa, Appl. Phys. Lett. **79**, 725 (2001).

Full References

1. X. Lei, B. C. Wang, V. Baby, I. Glesk, and P. R. Prucnal, "All-optical data format conversion between RZ and NRZ based on a Mach-Zehnder interferometric wavelength converter," IEEE Photo Techno Lett **15**, 308-310 (2003).
2. H. Chi, Z. Li, X. Zhang, S. Zheng, X. Jin, and J. P. Yao, "Proposal for photonic quantization with differential encoding using a phase modulator and delay-line interferometers," Opt Lett **36**, 1629-1631 (2011).
3. R. Yang, Y. S. Yu, Y. Xue, C. Chen, Q. D. Chen, and H. B. Sun, "Single S-tapered fiber Mach-Zehnder interferometers," Opt Lett **36**, 4482-4484 (2011).
4. Y. Xu, P. Lu, Z. Qin, J. Harris, F. Baset, P. Lu, V. R. Bhardwaj, and X. Bao, "Vibration sensing using a tapered bend-insensitive fiber based Mach-Zehnder interferometer," Opt Express **21**, 3031-3042 (2013).
5. J. Zhou, C. Liao, Y. Wang, G. Yin, X. Zhong, K. Yang, B. Sun, G. Wang, and Z. Li, "Simultaneous measurement of strain and temperature by employing fiber Mach-Zehnder interferometer," Opt Express **22**, 1680 (2014).
6. L. V. Nguyen, D. Hwang, S. Moon, D. S. Moon, and Y. Chung, "High temperature fiber sensor with high sensitivity based on core diameter mismatch," Opt Express **16**, 11369-11375 (2008).
7. H. Fu, X. Shu, A. Zhang, W. Liu, L. Zhang, S. He, and I. Bennion, "Implementation and Characterization of Liquid-Level Sensor Based on a Long-Period Fiber Grating Mach-Zehnder Interferometer," IEEE Sens J **11**, 2878-2882 (2011).
8. H. Y. Choi, M. J. Kim, and B. H. Lee, "All-fiber Mach-Zehnder type interferometers formed in photonic crystal fiber," Opt Express **15**, 5711-5720 (2007).
9. Y. Jung, S. Lee, B. H. Lee, and K. Oh, "Ultracompact in-line broadband Mach-Zehnder interferometer using a composite leaky hollow-optical-fiber waveguide," Opt Lett **33**, 2934 (2008).
10. Y. Xue, Y. S. Yu, R. Yang, C. Wang, C. Chen, J. C. Guo, X. Y. Zhang, C. C. Zhu, and H. B. Sun, "Ultrasensitive temperature sensor based on an isopropanol-sealed optical microfiber taper," Opt Lett **38**, 1209-1211 (2013).
11. D.-W. Duan, Y.-J. Rao, L.-C. Xu, T. Zhu, D. Wu, and J. Yao, "In-fiber Mach–Zehnder interferometer formed by large lateral offset fusion splicing for gases refractive index measurement with high sensitivity," Sensors and Actuators B: Chemical **160**, 1198-1202 (2011).
12. L. Mao, P. Lu, Z. Lao, D. Liu, and J. Zhang, "Highly sensitive curvature sensor based on single-mode fiber using core-offset splicing," Optics & Laser Technology **57**, 39-43 (2014).
13. P. Minkyu, L. Sejin, H. Woosung, K. Dae-Kyu, S. Woojin, S. Ik-Bu, and O. Kyunghwan, "Ultracompact Intrinsic Micro Air-Cavity Fiber Mach-Zehnder Interferometer," IEEE Photo Techno Lett **21**, 1027-1029 (2009).
14. Y. Wang, M. Yang, D. N. Wang, S. Liu, and P. Lu, "Fiber in-line Mach-Zehnder interferometer fabricated by femtosecond laser micromachining for refractive index measurement with high sensitivity," J Opt Soc Am B **27**, 370 (2010).
15. K. M. Davis, K. Miura, N. Sugimoto, and K. Hirao, "Writing waveguides in glass with a femtosecond laser," Opt Lett **21**, 1729 (1996).
16. H. Zhang, S. M. Eaton, J. Li, and P. R. Herman, "Femtosecond laser direct writing of multiwavelength Bragg grating waveguides in glass," Opt Lett **31**, 3495-3497 (2006).
17. L. A. Fernandes, J. R. Grenier, P. R. Herman, J. S. Aitchison, and P. V. Marques, "Femtosecond laser fabrication of birefringent directional couplers as polarization beam splitters in fused silica," Opt Express **19**, 11992-11999 (2011).
18. T. Kondo, S. Matsuo, S. Juodkazis, and H. Misawa, "Femtosecond laser interference technique with diffractive beam splitter for fabrication of three-dimensional photonic crystals," Appl Phys Lett **79**, 725 (2001).